DWI Study

Chase Junge[1]

[1]BYU Neuroimaging Course

April 9, 2018

Introduction

Alzheimer's disease (AD) is a devastating neurodegenerative disease that is believed to affect over 30 million people worldwide, including 5.3 million Americans (Alzheimers, 2015) It is the leading cause of dementia in the world and has a 100% mortality rate, mostly through related health deterioration. The costs of AD are staggering and continue to grow with a large amount of the United States population, the Baby Boomers, approaching the standard age of onset. In 2014, the cost of AD-related care for both families and Medicare was estimated at $217 billion. With the costs and incidence of AD expected to grow as more Americans age, the need for greater understanding and treatment of AD is paramount.

Extensive research has been done into possible causes of AD. AD symptomology includes: memory loss that disrupts daily life, a decline in problem-solving ability, confusion related to time and place, visuo-spatial deficits, decreased judgment, and marked changes in personality and mood varying from apathy to increased aggression. Such symptoms are varied in presentation and severity and are difficult to use as a direct diagnosis. Both modern neuroimaging methods and post-mortem studies have revealed several trends in AD pathology. Key changes within the central nervous system include the aggregation of beta-amyloid plaques, which are insoluble protein tangles, outside of neurons and the buildup of the neuronal protein, tau, within neurons. These combined protein buildups cause significant disruption in the brain. Beta-amyloid plaques may interfere with neuronal communication at synapses and may choke neurons from the exterior. Interior tau buildups can prevent the correct movement of essential materials from soma to dendrite and axons within individual neurons which can lead to neuronal death. Death in one neuron can lead to cascades of nearby neuronal death, and thus, the cycle of neurodegeneration continues in the disease. Much research has been done into individual mutations within these proteins that build up and some mutations have been identified as increased risk factors for individuals, though little progress has been made in identifying a single mutation responsible or a way to prevent the accumulation of such tangles. Such changes often begin years before symptoms appear and by the time symptoms appear, there has been little success in slowing the progression of AD.

This study aims to understand the deterioration involved within white matter tracts in the brain. All participants were imaged for both T1 (structural) and diffusion weighted (water movement within white matter) sequences. The focus will be on changes in diffusion patterns in AD patients against healthy controls. Several common measures will be analyzed to determine a potential loss of white matter integrity in AD patients as compared to their healthy controls. Fractional anisotropy, mean diffusivity, radial diffusivity, and axial diffusivity measures will all be calculated in order to determine the health of white matter tracts within AD individuals. It is hypothesized that AD patients will show decreased white matter integrity through these measures and through overall white matter tract integrity. Temporal lobe atrophy has also been linked to AD, we hypothesize that overall volumes in many parts of the temporal lobe and limbic region

will be significantly decrease in AD patients as compared to healthy controls.

Methods

Participant Demographics

A total of 26 patients were imaged as part of the European DTI Study on Dementia. Of the 26 participants, 10 were diagnosed with Alzheimer's disease while the other 16 were age-matched control. The age range in the study was from 53 to 81 years old. 17 females and 9 males participated in the study with the genders and education levels being evenly distributed between experimental and control groups. All participants took the Mini-Mental State Examination in order to quantify the level of dementia or confirm their healthy mental state.

T1 Scan Parameters

The scanner utilized for the study was a Siemens TrioTim 3.0T scanner. The parameters to acquire the T1 images done using Magnetization Prepared Rapid Acquisition Gradient Echo (MPRAGE) scan parameters. The echo time was 2.15 ms with an inversion time of 1100 ms and a slice thickness of 1 mm. A flip angle of 12 degrees was used with an acquisition matrix of 256 x 256 mm.

DWI Scan Parameters

The parameters utilized for acquired the diffusion weighted images were as follows. T2 images were taken by adding magnetic field gradient pulses to a conventional spin echo pulse. The echo time utilized was 94 ms and the inversion time was 1750 ms with a 90 degree flip angle. An acquisition matrix of 104 x 104 mm was used with a slice thickness of 2 mm. These gradient pulses were focused at varying coordinates along the x, y, and z axes in order to acquire a spherical image. The bval of the DTIs were as follows:

0 0 0 0 0 0 0 0 1000 1000 1000 1000 1000 1000 1000 1000 1000 1000 1000 1000 1000 1000 1000 1000 1000 1000 1000 1000 1000 1000 1000 1000 1000 1000 1000 1000 1000 1000 1000 1000 1000 1000 1000 1000 1000 1000 1000 1000 1000 1000 1000 1000 1000 1000 1000 1000 1000 1000 1000 1000 1000 1000 1000 1000

All data processing was completed on the Mary Lou Fulton Supercomputer at Brigham Young University. The Fulton Supercomputing Lab maintains 21,552 CPU cores and 972 compute nodes, all running Red Hat Enterprise Linux 6.6. For more information and all technical details of the supercomputing system please refer to: https://marylou.byu.edu/documentation/resources.

T1 Preprocessing Steps

In order to standardize the images that were obtained, a series of preprocessing steps were necessary. The first step was to convert the images obtained by the MRI scanner in a DICOM format into a NIfTI format that enables editing and normalization through the dcm2nii program (NITRC, Chris Rorden) which was downloaded from the following URL:https://www.nitrc.org/frs/?group_id=880. The version of dcm2niix utilized in this study was version v1.0.20170821 and the code entered was as follows:

```
~/apps/dcm2niix/bin/dcm2niix -o ${DATA_DIR}/t1/ -f t1 -x y -z n ${DATA_DIR}/DICOM/mprage/
~/apps/dcm2niix/bin/dcm2niix -o ${DATA_DIR}/raw/ -f dti -z y ${DATA_DIR}/DICOM/diff/
```

In addition to converting formats, the -x option of the code allowed the program to reorient and crop the images to a more anatomical position. Due to different scanning parameters, this reorientation brings all scans to have the same directions for x, y, and z coordinates and aligns it as if all scans had been taken from a coronal perspective. The x coordinates go from left to right in a negative to positive direction, y becomes positive moving posterior, and z coordinates become more positive moving superior. The cropping is also crucial in order to remove excess space from the field of view. The -z flag is the option to zip or compress the file. The -f flag shows the pathway to the image to be processed.

The next step in image preprocessing involved aligning the scans along the anterior and posterior commissures. Such an alignment is necessary due to the varied positioning of the subjects within the magnetic field of the scanner. The program utilized, acpcdetect, is part of the Automatic Registration Toolbox program (NITRC) and was downloaded from the following URL: https://www.nitrc.org/frs/?group_id=90. The version of acpcdetect utilized was 2011-04-05. The code utilized was as follows:

```
~/apps/art/acpcdetect -M -o ${DATA_DIR}/t1/acpc.nii -i ${DATA_DIR}/t1/t1_Crop_1.nii
```

The -M option commands the program to make the midpoint between AC and PC the center of the output field of view. This alignment in addition to reorientation done in the dcm2niix program allows all subjects to have an identical orientation in the FOV and midline.

After aligning the images along the x-,y-, and z- planes in this manner, it was necessary to correct the bias field and remove irregularities in contrast and shading within each individual image. Along with making the image visually more uniform, this process also removes error when applying tissue segmentation techniques to the images. The program Advanced Normalization Tools (ANTs) (STNAVA) (STNAVA) was used for this process and was downloaded from the following URL: http://stnava.github.io/ANTs/. The version of ANTs utilized for the study was ANTS Version 2.2.0.dev1-g8479e and the code was as follows:

```
~/apps/ants/bin/N4BiasFieldCorrection -v -d 3 -i /
${DATA_DIR}/t1/acpc.nii -o /
${DATA_DIR}/t1/n4.nii.gz -s 4 -b [200] -c [50x50x50x50,0.000001]
```

The -d flag signifies that the input image was three dimensional, the -s flag is a shrink factor of 4 which is the most commonly accepted factor as part of the preprocessing process. The -b flag is bspline-fitting and 200 is also a commonly accepted quantity for such a study. The final flag -c is the convergence or the number of iterations run by the program, 50 being a commonly used value.

After this step was completed, the final remaining step in image preprocessing was to resample all images to have a voxel volume of 1 mm isotropic. This was done using the software Convert3D (ITKsnap) which was downloaded from the URL: http://www.itksnap.org/pmwiki/pmwiki.php?n=Downloads.C3D. The version of Convert3D utilized in this study was 1.1.0. The program was run with the following code:

```
~/apps/c3d/bin/c3d ${DATA_DIR}/t1/n4.nii.gz -resample-mm 1x1x1mm -o ${DATA_DIR}/t1/resampled.nii.gz
```

In order to facilitate the preprocessing process, these four steps were combined into a script that contained all of the codes in order. This in turn was added to a secondary script that ran all participant images through the preprocessing process.

Template Creation

It was necessary to build a population template in this study in order to have a baseline comparison for all statistical analyses. The construction of a population template was done in two steps. First, an affine transformation was done on all participant T1 scans in order to construct a crude initial template. The purpose of the crude template was to place all participant scans into one computer-generated scan with the focus on whole brain structures rather than a voxel-by-voxel construction. All participant images files were previously copied into a data directory within the EDSD parent directory. The ANTs build template program then used all participant images within the directory to build a single template in common space using affine registration. Thus, the input for this program was all participants within the study and the output was a single, crude affine-registered template that would be further refined. The code utilized to run the affine transformation was as follows:

```
buildtemplateparallel.sh \
-d 3 \
-m 1x0x0 \
-o pt1 \
-c 5 \
img*.nii.gz
```

The -d flag is for the image being 3 dimensional, the -m is for max iterations, and -c is the convergence threshold, which is commonly set to 5 in all template generation using the ants program. The img*.nii.gz was the input files, directing the program to utilize all participant scans contained within the directory.

The next step was to run a diffeomorphic transformation on all participant scans to create a refined template. While running this program, all parameters were the same as in the affine transformation with the addition of the -z flag which told the program to compare what it was building to the previously generated crude template. Using the crude template as a backdrop, the diffeomorphic transformation could build a refined voxel-by-voxel template using the crude affine template as a type of scaffolding and framework for the final product. The code was as follows:

```
buildtemplateparallel.sh \
-d 3 \
-z ~/templates/class/pt1template.nii.gz \
-o pt2 \
-c 5 \
img*.nii.gz
```

Freesurfer

Cortical reconstruction and volumetric segmentation was performed with the Freesurfer image analysis suite, which is documented and freely available for download online (http://surfer.nmr.mgh.harvard.edu/). The technical details of these procedures are described in prior publications (Dale et al., 1999; Dale and Sereno, 1993; Fischl and Dale, 2000; Fischl et al., 2001; Fischl et al., 2002; Fischl et al., 2004a; Fischl et al., 1999a; Fischl et al., 1999b; Fischl et al., 2004b; Han et al., 2006; Jovicich et al., 2006; Segonne et al., 2004, Reuter et al. 2010, Reuter et al. 2012). Briefly, this processing includes motion correction and averaging (Reuter et al. 2010) of multiple volumetric T1 weighted images (when more than one is available), removal of non-brain tissue using a hybrid watershed/surface deformation procedure (Segonne et al., 2004), automated Talairach transformation, segmentation of the subcortical white matter and deep gray matter

volumetric structures (including hippocampus, amygdala, caudate, putamen, ventricles) (Fischl et al., 2002; Fischl et al., 2004a) intensity normalization (Sled et al., 1998), tessellation of the gray matter white matter boundary, automated topology correction (Fischl et al., 2001; Segonne et al., 2007), and surface deformation following intensity gradients to optimally place the gray/white and gray/cerebrospinal fluid borders at the location where the greatest shift in intensity defines the transition to the other tissue class (Dale et al., 1999; Dale and Sereno, 1993; Fischl and Dale, 2000). Once the cortical models are complete, a number of deformable procedures can be performed for further data processing and analysis including surface inflation (Fischl et al., 1999a), registration to a spherical atlas which is based on individual cortical folding patterns to match cortical geometry across subjects (Fischl et al., 1999b), parcellation of the cerebral cortex into units with respect to gyral and sulcal structure (Desikan et al., 2006; Fischl et al., 2004b), and creation of a variety of surface based data including maps of curvature and sulcal depth. This method uses both intensity and continuity information from the entire three dimensional MR volume in segmentation and deformation procedures to produce representations of cortical thickness, calculated as the closest distance from the gray/white boundary to the gray/CSF boundary at each vertex on the tessellated surface (Fischl and Dale, 2000). The maps are created using spatial intensity gradients across tissue classes and are therefore not simply reliant on absolute signal intensity. The maps produced are not restricted to the voxel resolution of the original data thus are capable of detecting submillimeter differences between groups. Procedures for the measurement of cortical thickness have been validated against histological analysis (Rosas et al., 2002) and manual measurements (Kuperberg et al., 2003; Salat et al., 2004). Freesurfer morphometric procedures have been demonstrated to show good test-retest reliability across scanner manufacturers and across field strengths (Han et al., 2006; Reuter et al., 2012).

In addition, the Freesurfer option to segment and analyze hippocampal subfields was run. This was done due to the nature of the research, Alzheimer's has been clearly connected with hippcampal atrophy and loss and a Freesurfer analysis was run in order to detect the nature and extent of atrophy in AD participants. The Freesurfer code run was as follows:

```
/freesurfer/bin/recon-all \
-subjid ${1} \
-i /fslhome/${var}/compute/images/EDSD/${1}/t1/resampled.nii.gz \
-wsatlas \
-all \
-hippocampal-subfields-T1 \
-sd /fslhome/${var}/compute/analyses/EDSD/mindboggle/freesurfer_subjects/
```

ANTs Cortical Thickness

The program Advanced Normalization Tools (ANTs) (STNAVA) (STNAVA) was used for this process and was downloaded from the following URL: http://stnava.github.io/ANTs/. The version of ANTs utilized for the study was ANTS Version 2.2.0.dev1-g8479e. The ANTs cortical thickness pipeline involves 4 steps: initial N bias field correction on input MRI, brain extraction using both segmentation and template-based strategies, alternation between prior-based segmentation and pure tissue, cortical thickness estimation, and optional normalization to a chosen template (Tustison et al., 2014). The N4 bias field correction is used to eliminate low intensity levels throughout the images caused by a variety of issues in scanning. Such intensity levels, if left uncorrected, may lead to errors in both thickness calculations and cortical parcellations. The brain extraction involves using both templates and image registration to build an accurate brain mask which is used for subsequent comparisons. The third step involves seprating the different tissue types which are CSF, gray matter, white matter, deep gray matter, brain stem, and cerebellum. The fourth step involves

intensive algorithms within the ANTs program that determine the cortical thickness at each point on the cortex surface. The final step is optional and can be used to compare for significant differences in subject cortical thickness as compared to a population template.

In the ANTs Cortical Thickness pipeline used in this study, the Open Access Series of Imaging Studies (OASIS) template was used. This template was derived from a data set of 433 T1 images with 120 excluded due to possible Alzheimer deterioration and repeats. The final 313 scans included participants between 18 and 96 years of age. The OASIS template was utilized due to it being the only ANTs pipeline accepted by the Mindboggle software.

The ANTs code utilized in this study was as follows:

```
ants/bin/antsCorticalThickness.sh \
-d 3 \
-a ${DATA_DIR}/t1/resampled.nii.gz \
-e ${TEMPLATE_DIR}/T_template0.nii.gz \
-t ${TEMPLATE_DIR}/T_template0_BrainCerebellum.nii.gz \
-m ${TEMPLATE_DIR}/T_template0_BrainCerebellumProbabilityMask.nii.gz \
-f ${TEMPLATE_DIR}/T_template0_BrainCerebellumExtractionMask.nii.gz \
-p ${TEMPLATE_DIR}/Priors2/priors%d.nii.gz \
-q 1 \
-n 6 \
-x 6 \
-o ~/compute/analyses/EDSD/mindboggle/ants_subjects/${1}/
```

The -n flag signals the program to run 6 iterations of the N4 bias field correction and the -x flag signals for 6 iterations of the cortical thickness calculations. Both are slightly higher than is standard but were believed to be necessary for accurate input into Mindboggle.

Mindboggle

The program Mindboggle was utilized in this study to more accurately label and measure brain areas and volume. The version of Mindboggle utilized was 1.2.2 and was downloaded onto the Fulton Supercomputing Lab from this URL: http://mindboggle.readthedocs.io/en/latest/#installation. The Mindboggle program takes the outputs from Freesurfer and ANTs Cortical Thickness and runs it through its own algorithms to refine each program's process and output. The data output by Mindboggle includes hybrid gray/white matter segmentation, advanced labelling of images, calculation of volume and thickness of cortical labels, extract cortical surface features including folds, sulci, and fundi, and computes statistics for each labelled area. The code to run Mindboggle was as follows:

```
singularity run --bind /panfs/pan.fsl.byu.edu/mapping/usr/scr/$var:/home/jovyan/work \
    /apps/singularity/container/mindboggle.img \
    /home/jovyan/work/images/EDSD/$i/t1/resampled.nii.gz \
    --id $i \
    --plugin MultiProc \
```

```
    --plugin_args "dict(n_procs=2)" \
    --fs_openmp 5 \
    --ants_num_threads 5 \
    --mb_num_threads 10 \
    --out /home/jovyan/work/analyses/EDSD/mindboggle/
done
```

TBSS Processing

The next step in preprocessing involved processing the diffusion-weighted images obtained in the study. All DWI preprocessing was done using FSL version 5.0.7 downloaded from the URL: http://fsl.fmrib.ox.ac.uk/fsl/fslwiki/FslInstallation. FSL does several steps in its preprocessing stream including skull stripping, eddy current correction, and adjusting for head motion in the scanner. In addition to this, the program uses the fractional anisotropy, axial diffusivity, radial diffusivity, and mean diffusivity maps and matches them voxel by voxel to a tensor model. All maps were matched to a large population template rather than a template generated from this experiment's population. The code was as follows:

```
cd ~/compute/images/EDSD/${1}/raw/
eddy_correct dti.nii.gz data.nii.gz 0
bet data data_brain -f 0.25 -g 0 -m
dtifit --data=data.nii.gz --out=dti --mask=data_brain_mask.nii.gz --bvecs=dti.bvec --bvals=dti.bval --s
```

The eddy correct in the code is simply to register the DWI image to the non-DWI image using linear transformation. This is done to remove any head movement artifacts throughout the DWI imaging sequence. The bet flag is brain extraction with skull strip. The -f flag utilized is a commonly used value in order to give a wide enough image without cutting too much or too little skull from the inputted images. The dtifit flag is where FA, RD, MD, and AD whole-brain diffusion tensors are calculated.

From this point, the following TBSS preprocessing was done in 4 separate steps. The first step was to process all of the FA images, slice by slice and the code was as follows:

```
cd ~/compute/analyses/EDSD/TBSS/
tbss_1_preproc \*.nii.gz
```

The second step was to diffeomorphically register all FA images to standard space by comparison to a standard template. The code was nearly identical to step 1 with the only change being the last line:

```
tbss_2_reg -T
```

The third step averages all participant FA images to a single image. It also skeltonizes that image, leaving only the core parts of the white matter tracts being measured. Again, it has only one change in the last line of code being:

```
tbss_3_postreg -S
```

Step 4 is simply projecting each participant FA data onto the mean FA skeleton in order to normalize everything. The code was again similar to the past 3 with the exception of the past line. The option .2 was selected as the most common number utilized in TBSS processing.

```
tbss_4_prestats 0.2
```

These same processes were rerun with all participants' AD, MD, and RD data and was able to be run all in one step using the initial code given, changed to reflect the type of data being run.

Voxelwise Statistics

In order to analyze the data given by the TBSS pipeline, voxelwise statistics were run using the FSL randomize program. In order to run these statistics, an initial matrix was generate in order to identify which participants were part of the AD group and which were part of the healthy controls in order for the randomize program to run calculations only against the opposite group. This matrix simply was a 2x26 matrix with a 1 0 designation for AD patients and a 1 0 designation for controls. A contrast matrix was also created in order to tell the program which parameters to test for. A 4x2 matrix was run in order to get results for mean AD, mean HC, AD vs HC and HC vs AD. Following the creation of the design and contrast matrices, the program was run with the following code:

```
randomise -i ${1} -o ${2} -m mean_FA_skeleton_mask /
-d design.mat -t design.con -n 5000 --T2 -V>
```

All computations run by the program compare back to the mean FA skeleton which was created as part of the TBSS pipeline. 5000 iterations were run in order to ensure accuracy and power of resulting statistics. From here, a short code was run in order to highlight only significant areas in FA, MD, AD, and RD for the AD vs HC and HC vs HC graphs. The code was as follows:

```
tbss_fill tbss_FA_tfce_corrp_tstat3 0.95 mean_FA tbss_FA_tfce_corrp_tstat3_fill
tbss_fill tbss_FA_tfce_corrp_tstat4 0.95 mean_FA tbss_FA_tfce_corrp_tstat4_fill
```

At this point, individual heat maps showing significant changes in RD, AD, FA, and MD were visualized using Mango and the results can be found in the results below.

Tractography

A different preprocessing streamline was necessary before running our global tractography pipeline. All preprocessing steps were completed using MATLAB. Tractography was selected for this study due to its high level of accuracy in identifying white matter tracts in the brain as compared to other common methods. Though accurate, tractography has two major limitations. The first being the inability to do whole brain analyses. Instead, tractography is limited to a delineated area of white matter tracts where all computations are run and analyzed. The second being the time-consuming nature to do thorough analysis of the most common white matter tracts in the brain. Despite the limitations, certain areas of the brain were processed using tractography in order to diversify and confirm findings. As part of the preprocessing through MATLAB, six individual outcomes are achieved. The first, all B0 images are average into a single B0 image in order to avoid misalignment. Second, standard eddy current corrections are calculated and fixed to adjust for movement within the scanner during the DWI image collection. Third, the DWI is aligned to the MNI image to more accurately align all structures within the natural space of the participant. Fourth, all DWIs are resampled to 2 mm isotropic for uniformity in future calculations. Fifth, bvec is correctly rotated and confirmed. Lastly, each voxel is assigned a tensor direction that will later be used in the tratography pipeline to determine the locations and boundaries of all white matter tracts within our ROI. The MATLAB code was as follows:

```
% Determine phase encode dir:
dwParams = dtiInitParams('rotateBvecsWithCanXform', 1, 'phaseEncodeDir', 2, 'clobber', 1);

% DTI preprocessing:
dtiInit(dtiFile, 'MNI', dwParams);

% Clean up files and exit:
movefile('dti_*', 'raw/');
movefile('dtiInitLog.mat', 'raw/');
movefile('ROIs', '*trilin');

exit;
```

Automated Fiber Quantification (AFQ)

The AFQ pipeline is a pipeline run through a MATLAB script that maps out the main fiber tracts of the brains. Initially, the pipeline does a global analysis and identifies all fiber tracts in each participant. Following this, each known fiber tract has a set starting and ending ROI in which all fiber tracts falling between the two ROIs are combined into known fiber tracts. The program then confirms the calculated fiber tracts against template values and against other participants in order to remove outliers. These confirmed fiber tracts are then further compared against a fiber tract probability map to ensure accuracy. The AFQ pipeline was then run a second time in order to complete the corpus collosum tracts as they cross hemispheres. Both parts of the AFQ code in MATLAB can be found below:

```
afq = AFQ_Create('sub_dirs', sub_dirs, 'sub_group', sub_group, 'showfigs', false);
[afq, patient_data, control_data, norms, abn, abnTracts] = AFQ_run(sub_dirs, sub_group, afq);
save(outname, 'afq');
```

Above was the first entrance of the participants through the AFQ pipeline. It is crucial before these participants are run to make a MATLAB matrix through a text editor in order to delineate the correct sub-directories for each participant and sub-groups for affected and control groups. These matrices were delineated in the above code as sub_dirs.mat and sub_group.mat respectively. Below is seen the second submission through the AFQ pipeline, with the only changes being the output of the first AFQ pipeline added and written over.

‘‘‘

afq = AFQ_SegmentCallosum(afq, 0) save(outname, ‘afq’);

Results

White Matter Integrity

In order to determine white matter integrity, the outputs from both the TBSS pipeline and AFQ analyses were used to determine areas of significantly decreased white matter integrity. First, the outputs from TBSS

were analyzed using voxelwise statistics (see methods) for areas of significantly increased levels of fractional anisotropy (FA), mean diffusivity (MD), axial diffusivity (AD), and radial diffusivity (RD). FA is measure of the freedom or restrictedness of diffusion in a certain area. High FA values are expected in healthy white matter due to the unidirectional diffusion (therefore high FA value) seen in health myelin. Lower FA values may show loss of white matter and myelin integrity as water is allowed to diffuse in different directions through deteriorated regions. Figure 4 shows the extensive regions of the brains in white healthy controls had higher FA values than those of AD patients. In each of the red regions, we can assume white matter deterioration in AD patients where FA values are significantly lower at a p=.05 level.

The other three measures: mean diffusivity, axial diffusivity, and radial diffusivity were expected to be higher in AD patients than in healthy controls. AD can be increased through axonal inflammation and other damages to white matter tracts, something expected to be seen more in AD than in controls. RD is simply expected to give opposite results than FA due to it showing diffusion in opposite directions, something that would normally only be seen in deteriorating WM. MD is more related is cell death than true WM integrity but is still expected to be higher in AD due to the cell death seen in the disease pathology.

As was expected AD (Figure 1), MD (Figure 2), and RD (Figure 3) all show significant areas of higher measurements in AD than in controls. As was stated above, we believe this to be a measure of loss of WM integrity in many areas of the brain. As can be seen in the figures, areas affected include the internal capsule, corpus callosum, corona radiata, and many other crucial WM tracts throughout the cerebrum and cerebellum. This suggests that AD is a global neurodegenerative disease that is not limited to specific areas of interest and could account for the white variety of symptoms and global deficits.

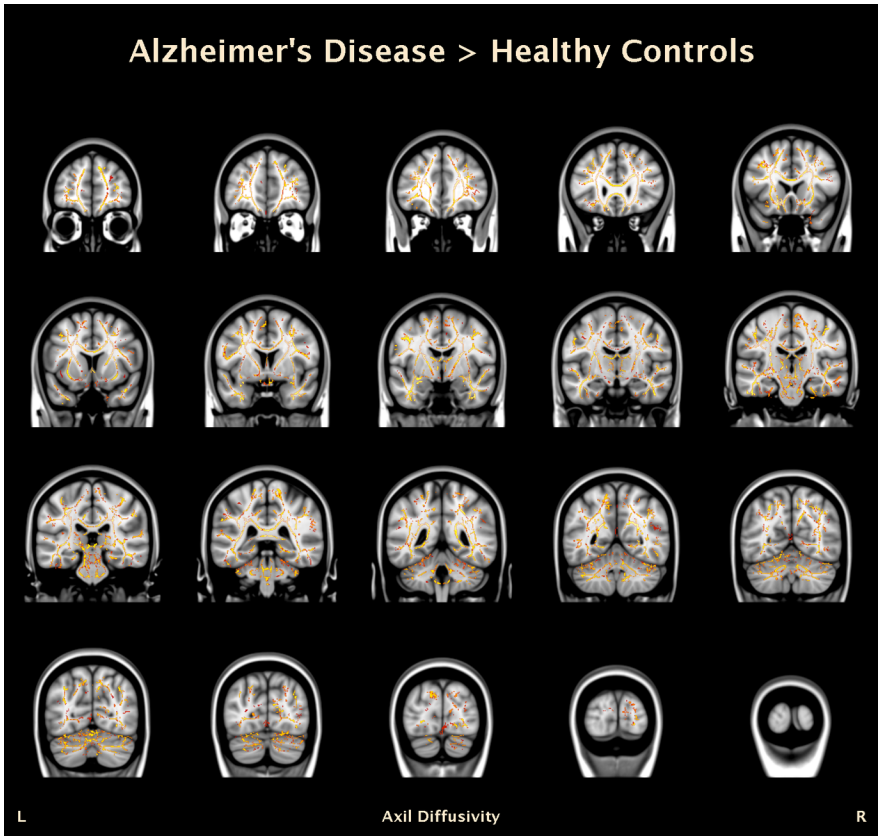

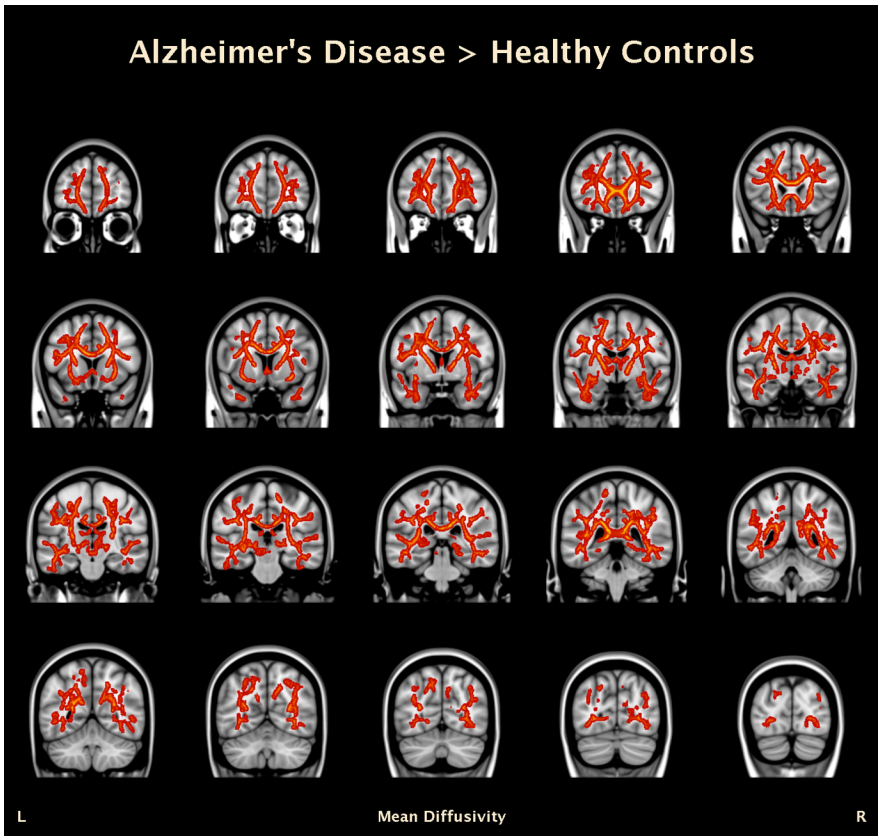

In addition to deterioration of WM tracts as seen through FA, MD, AD, and RD, we utilized the Freesurfer pipeline in order to measure volume loss in the temporal lobe and limbic regions in AD patients. We hypothesized that memory loss that is a key part of AD symptomology could be related to neuronal loss in the hippocampus and other surrounded regions implicated in memory. We believed that this neuronal loss would be manifested through volume loss in hippocampal regions. The results were measured through the Freesurfer hippocampal subfield command in the recon-all pipeline. The results were powerful and significant decreases were seen in AD patients in 21 of 25 areas examined. The areas that showed significant decreases in volume included right and left hippocampal tail, subiculum, CA1, presubiculum, fimbria, whole hippocampus, and various Brodmann areas within the hippocampal area. The only regions that didn't show significant decreases in volume were the right and left hippocampal fissure and parasubiculum. It is unknown why these regions are unaffected by AD pathology while all other areas in the region are heavily affected and should be an area of future research. Figures 5-10 shown below are a graphical representation of the most significant findings in key areas of the hippocampus and surrounding areas on both right and left sides. Volume decreases in the hippocampal tails are on average, over 150 mm^3 which are huge losses in a small region. Total hippocampal volume losses average over 1000 mm^3 or nearly a 33% loss of total hippocampal volume. Such results give strong implications in the severe memory decline seen in AD patients.

After obtaining significant results with WM integrity on a global scale and significant volume losses, we wanted to look into WM tract integrity in the key WM tracts in the limbic system. It is possible that the memory deficits seen in AD could be limited to degeneration in the hippocampus and surrounded areas or could be a combination with WM tract deterioration in the limbic area. Due to the key nature of the

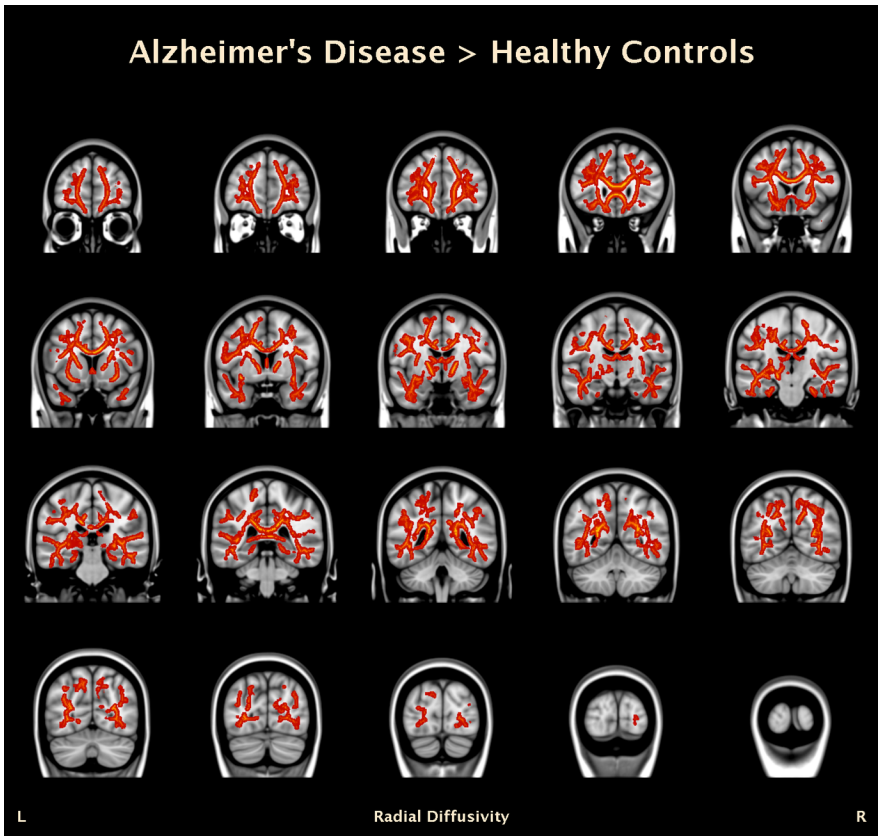

Cingulate Cingulum and Cingulum Hippocampus tracts in communication throughout the limbic area, we measured FA, AD, MD, and RD in these areas. The tracts as identified through AFQ were mapped through MATLAB and the results were relatively uniform as seen below.

As a whole, FA results were similar to those obtained in a global manner with TBSS analyses. On the whole, controls had a higher FA than AD participants showing slight deterioration in AD patients in key limbic WM tracts. These were seen most clearly in the right Cingulum Hippocampus and left Cingulum Cingulate though laterality differences were not well explained.

The MD results as shown above were much more conclusive. Significant differences exists throughout both WM tracts measured in MD, with AD showing higher measurements, suggesting loss of tract integrity. Such trends were identical in AD and RD graphs, and such were omitted in order to avoid repetition. The data is relatively clear in its results, for both the Cingulum Hippocampus and Cingulate Cingulum, key WM tracts in the limbic system, there is a marked decrease in tract integrity according to classical measurements. Such decreases in combination with the volume decreases seen in the hippocampus and surrounding regions suggest that AD affects both gray and white matter in the limbic system. Neurodegeneration in this regions measured by loss of WM integrity and volume loss could be a direct cause of the severe memory deficits seen in AD.

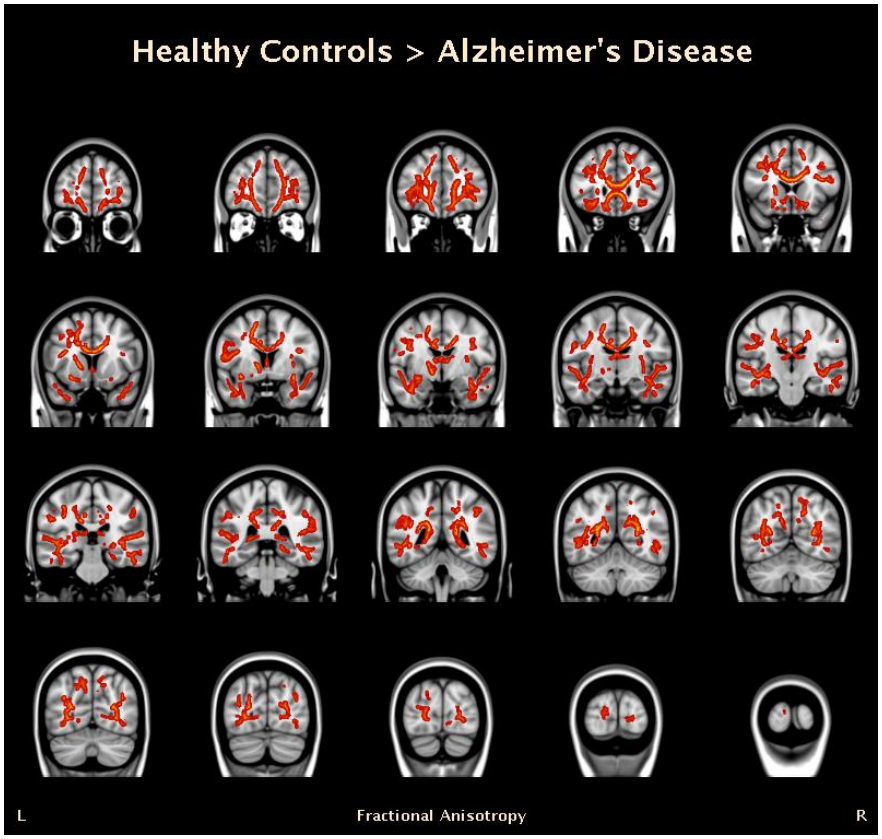

Figure 1: All subjects significant areas of statistical difference for FA, AD, MD, and RD

Discussion

As hypothesized, our data suggests both significant decreases in hippocampal and temporal lobe volume as well as significant loss of white matter integrity in various key white matter tracts. Volumetric data given by Freesurfer showed significant volume loss in all but 2 areas of the hippocampus measured. Such volume losses were not small, showing up to 33% volume loss in several key areas including total hippocampal volume. There volume losses could be a key part of the symptomology seen in AD, especially in the sharp decline in working, short term, and long-term memory that are common symptoms. Voxelwise statistics on global tractography showed trends in FA, AD, MD, and RD that suggest loss of WM integrity throughout the cingulate cingulum and cingulum hippocampus, two key WM tracts in the limbic system. Global statistics also showed significant decreases in WM integrity in various key WM tracts throughout the cerebrum, suggesting that neurodegeneration in AD is not limited to the limbic area.

These findings point us in specific directions for future study. Specifically, the cause of both volume loss and WM deterioration is still unknown. Several theories exist using the known pathology of the disease

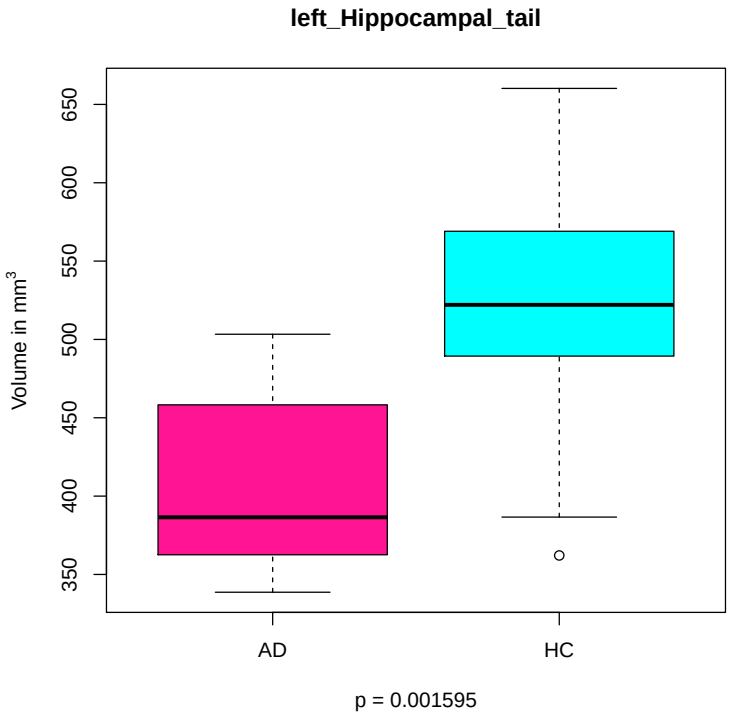

Figure 2: This is a caption

but currently, it is unknown how the biological markers of the disease interact with and affect the neurons damaged throughout the course of the disease.

There are certain limitations involved in this study, including sample size and technological limitations. The sample, drawn from a European population is limited in size and may reduce both the power of statistics run as well as the generalizability of the data to the general population. In addition, the programs utilized in this study have their own algorithms used to determine WM integrity, hippocampal volume, and many other processes run. Such algorithms may differ from those run in other studies which could lead to certain contradictions in data output. However, the author believes all programs were utilized with methods and settings in accordance with best practice as seen in the current literature and expects that such differences will be minimal.

References

A Klein, SS Ghosh, FS Bao, J Giard, Y Hame, E Stavsky, N Lee, B Rossa, M Reuter, EC Neto, A Keshavan. 2017. **Mindboggling morphometry of human brains**. *PLoS Computational Biology* 13(3): e1005350. doi:10.1371/journal.pcbi.1005350

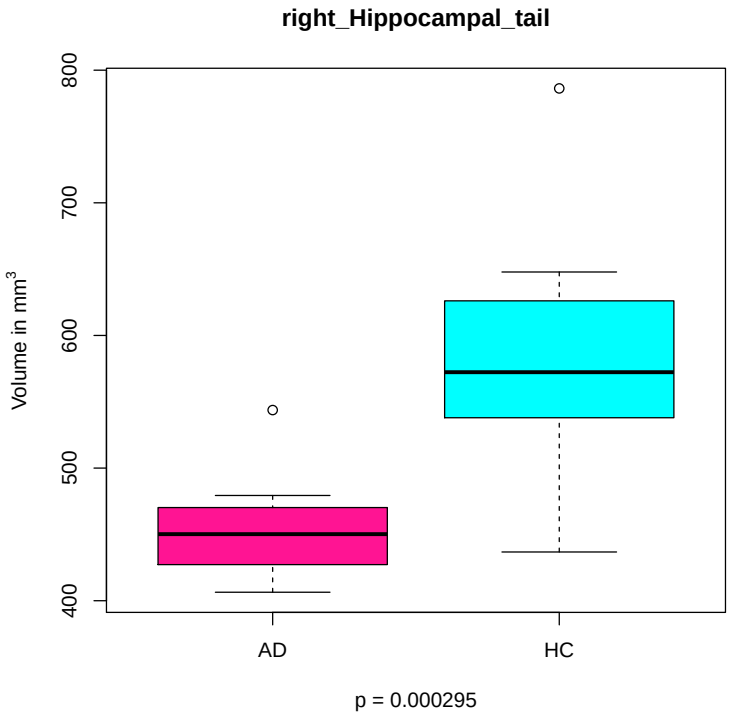

Figure 3: This is a caption

Alzheimers, A. (2015). 2015 alzheimer's disease facts and figures. *Alzheimer's & Dementia, 11*(3), 332-384. 10.1016/j.jalz.2015.02.003

Dale, A.M., Sereno, M.I., 1993. Improved localization of cortical activity by combining EEG and MEG with MRI cortical surface reconstruction: a linear approach. J Cogn Neurosci 5, 162-176.

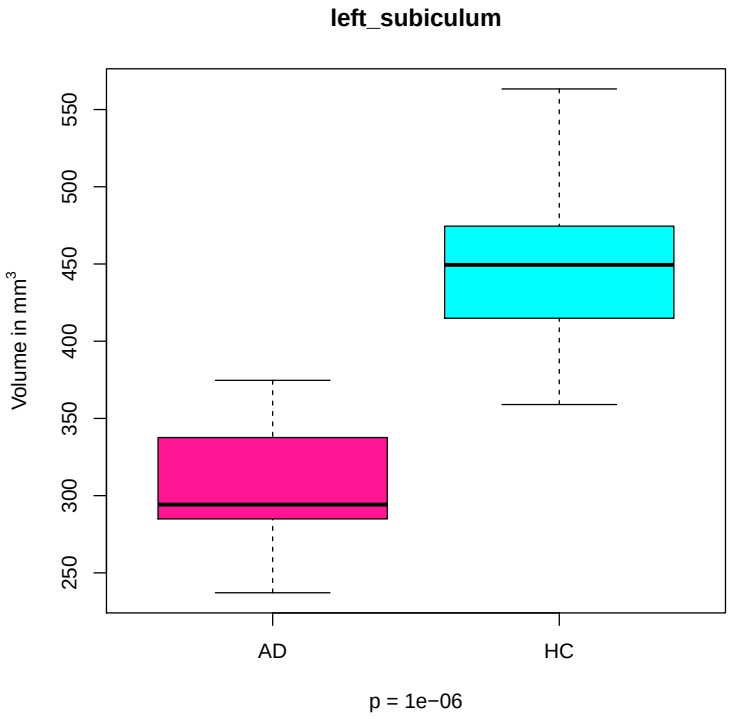

Figure 4: This is a caption

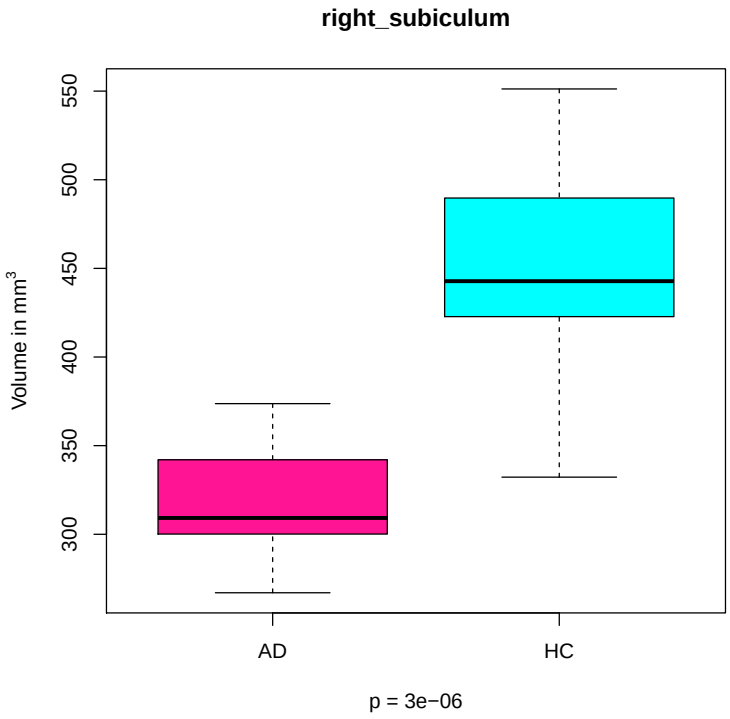

Figure 5: This is a caption

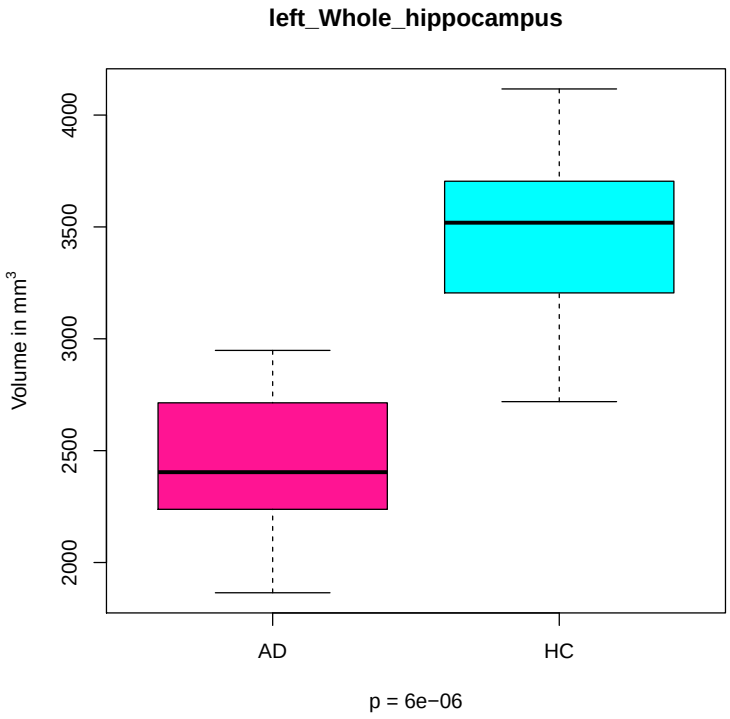

Figure 6: This is a caption

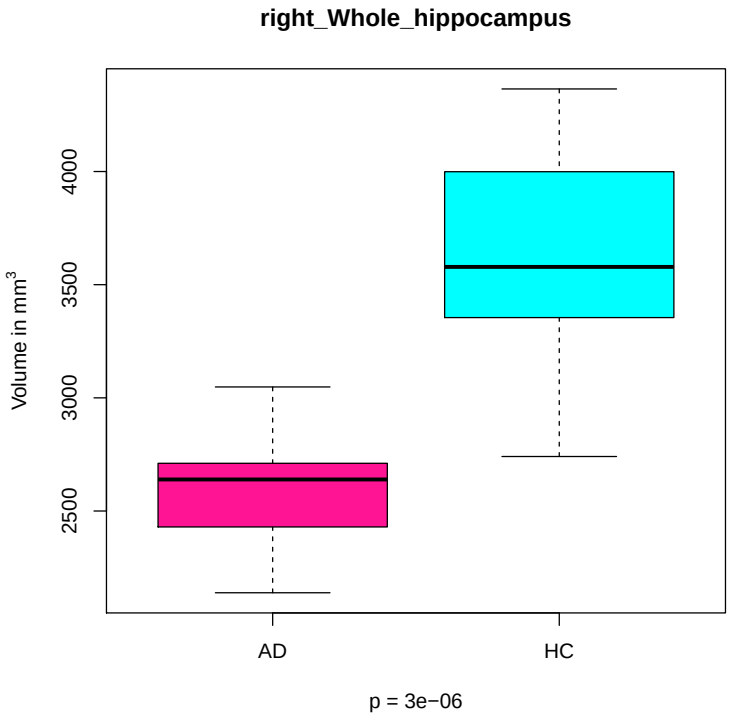

Figure 7: This is a caption

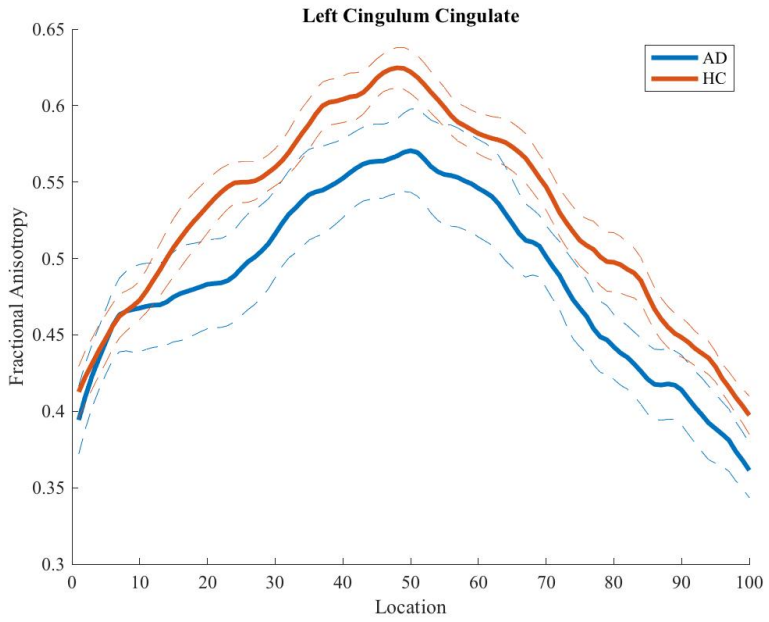

Figure 8: This is a caption

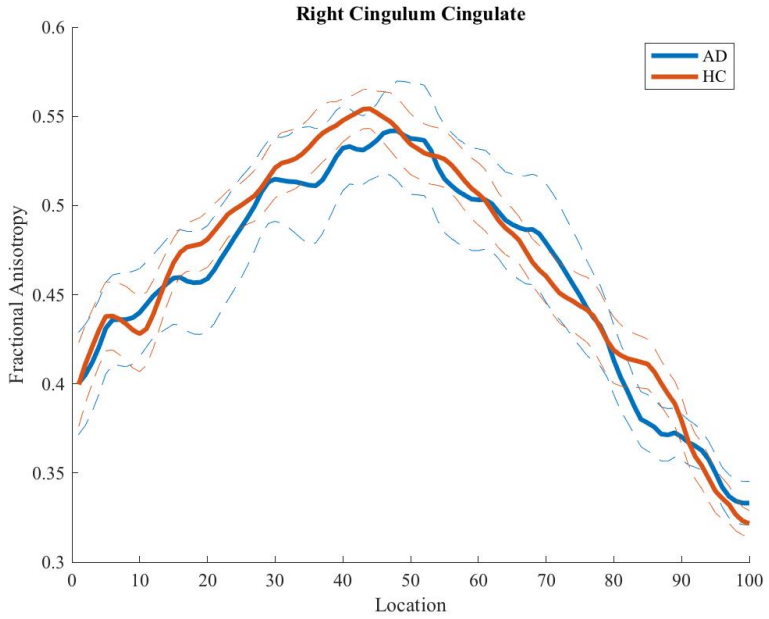

Figure 9: This is a caption

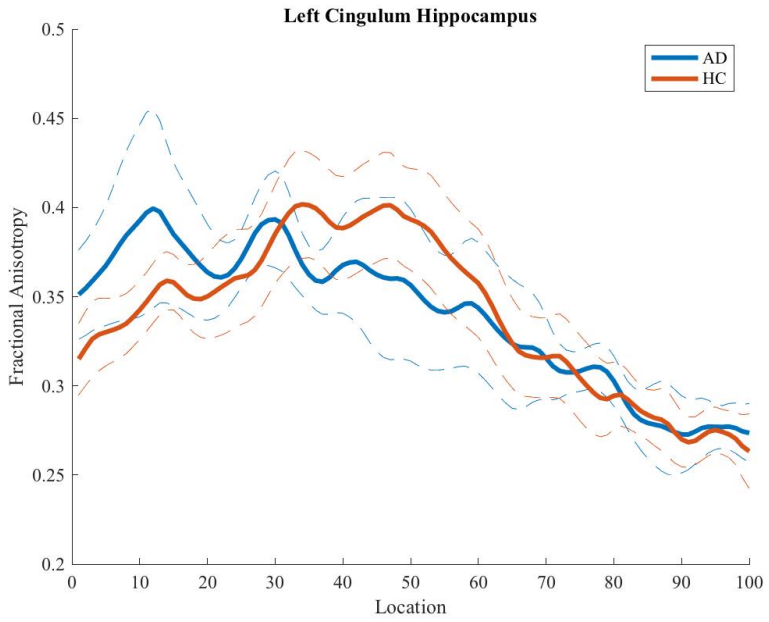

Figure 10: This is a caption

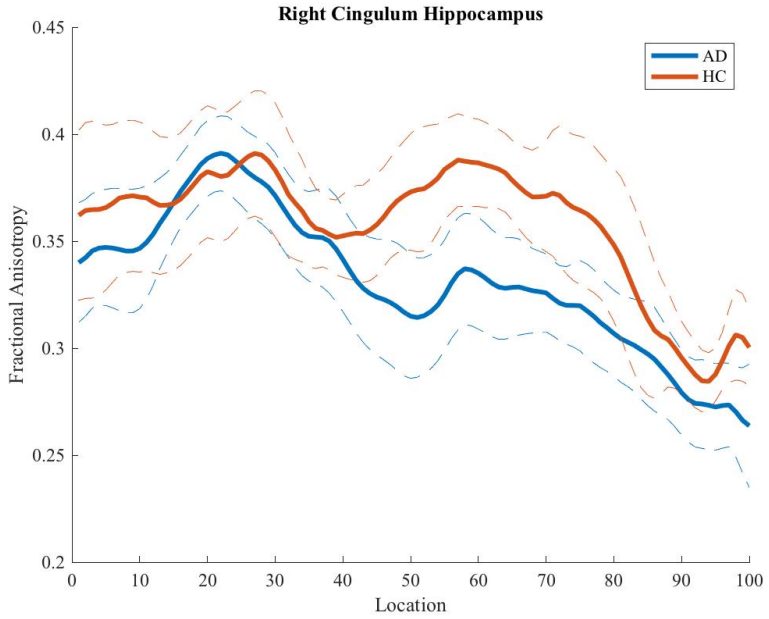

Figure 11: This is a caption

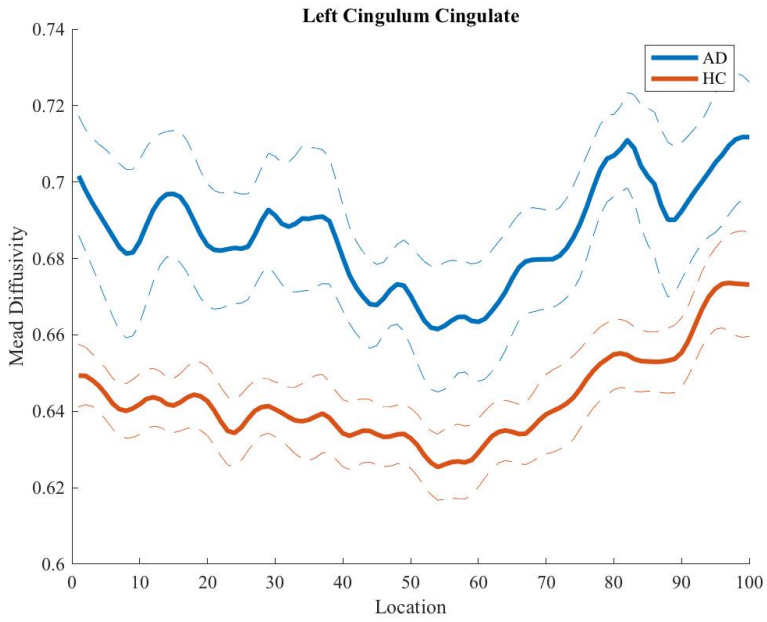

Figure 12: This is a caption

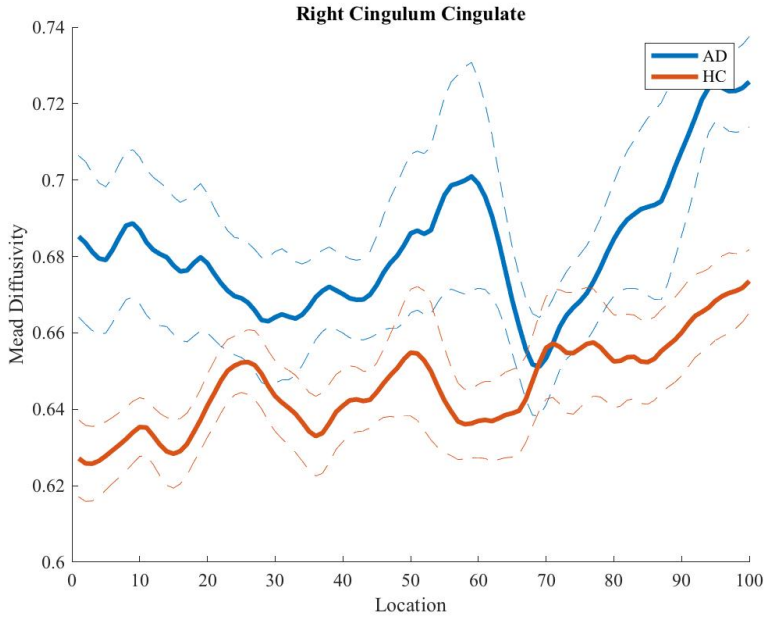

Figure 13: This is a caption

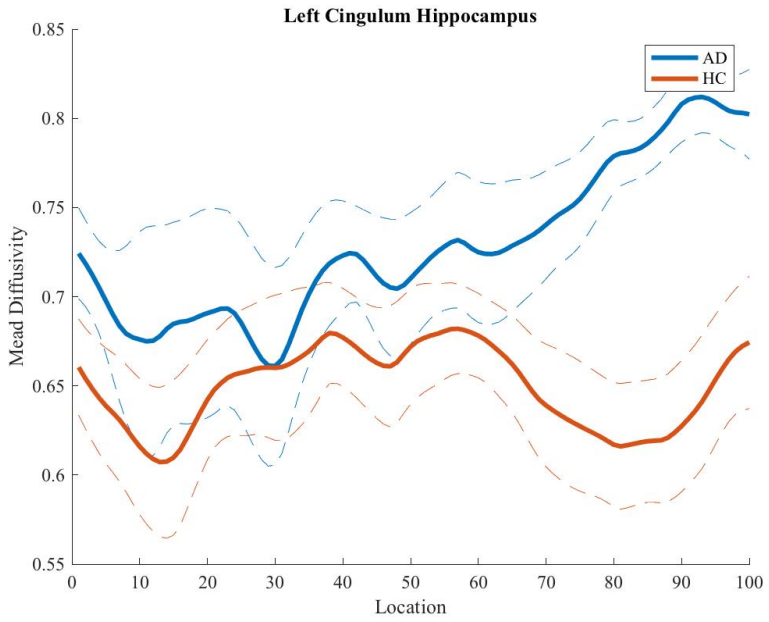

Figure 14: This is a caption

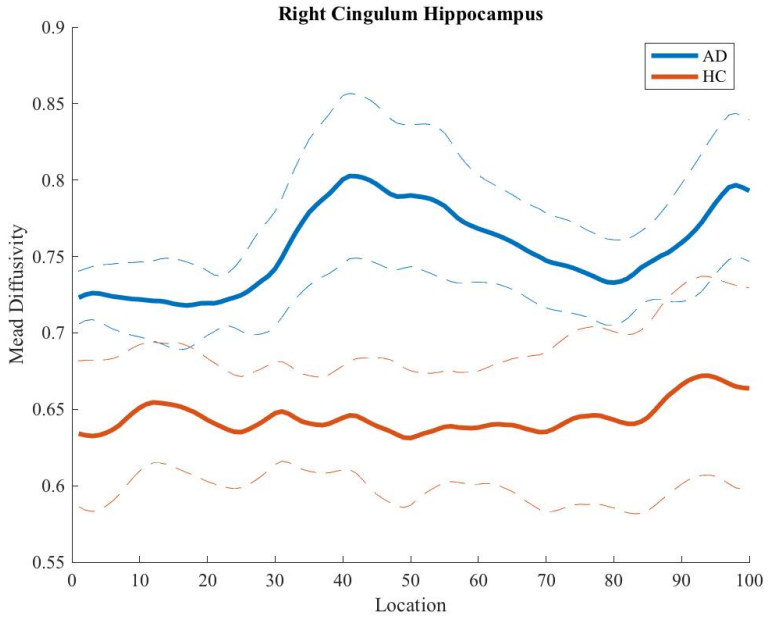

Figure 15: This is a caption